X-ray Raman Scattering Study of Aligned Polyfluorene

**Szabolcs Galambosi,*,† Matti Knaapila,‡ J. Aleksi Soininen,† Kim Nygård,†
Simo Huotari,§ Frank Galbrecht,‖ Ullrich Scherf,‖ Andrew P. Monkman,‡ and
Keijo Hämäläinen†**

*Division of X-ray Physics, Department of Physical Sciences, University of Helsinki, POB-64, FI-00014
University of Helsinki, Finland, Department of Physics, University of Durham, South Road, Durham
DH1 3LE, United Kingdom, European Synchrotron Radiation Facility, BP 220, F-38043 Grenoble,
France, and Fachbereich Chemie, Bergische Universität Wuppertal, Gauss Strasse 20,
D-42097 Wuppertal, Germany*

Received April 12, 2006; Revised Manuscript Received August 25, 2006

ABSTRACT: We present a nonresonant inelastic X-ray scattering study at the carbon K edge on aligned poly-[9,9-bis(2-ethylhexyl)-fluorene-2,7-diyl] and show that the X-ray Raman scattering technique can be used as a practical alternative to X-ray absorption measurements. We demonstrate that this novel method can be applied to studies on aligned π-conjugated polymers complementing diffraction and optical studies. Combining the experimental data and a very recently proposed theoretical scheme, we demonstrate a unique property of X-ray Raman scattering by performing the symmetry decomposition on the density of unoccupied electronic states into s- and p-type symmetry contributions.

Introduction

Various synchrotron radiation based inelastic X-ray scattering methods are now utilized in the study of electronic excitations. X-ray Raman scattering (XRS) is a technique analogous to Raman scattering in the optical region inasmuch as the energy difference of the incident and the scattered photon is an indication of an excitation within the target system. By using hard X-rays, an energy transfer of hundreds of electronvolts can easily be achieved, leading to core electron excitations in low-Z elements.

The method differs from X-ray absorption spectroscopy (XAS), or more specifically, from near-edge absorption fine structure spectroscopy (NEXAFS),[1] where the incident energy is tuned in the vicinity of an absorption edge, for example, around 285 eV in the case of carbon atoms. In an equivalent XRS experiment, the energy of the incident photon is typically around 10 keV, but the energy difference between the incident and scattered photons is around 285 eV. The nonresonant character of the core electron excitation leads to a relatively low cross section, which necessitates the use of synchrotron radiation to perform XRS experiments. However, by using hard X-rays, vacuum-sensitive samples can be measured as typically there is no need for a vacuum environment. Hard X-rays are bulk sensitive, which in many cases greatly simplifies the sample preparation and quality requirements. XRS is analogous to inner-shell electron energy loss spectroscopy (ISEELS).[2] However, the use of photons as the scattering probe instead of electrons leads to negligible multiple scattering problems, and again, no vacuum environment is needed.

In an absorption process, the energy loss and the photon momentum are interconnected, but in XRS, the momentum transfer during the scattering process can be varied independently of the energy transfer simply by varying the scattering angle. The cross section of XRS at low momentum transfers can be related to the same dipole matrix elements that determine the X-ray absorption process.[3] This feature has been successfully used in the field of hard condensed matter to probe the electronic excitations in various low-Z elements. XRS can be used as a substitute for extended X-ray absorption fine structure (EXAFS).[4,5] In anisotropic materials such as graphite, analogously to polarization dependent X-ray absorption, XRS may be used to probe the orientation of the density of electronic states.[6] The momentum transfer dependence of the XRS spectra has, for example, been used to study excitations at the fluorine K edge in LiF,[7] at the Be K edge in beryllium,[8] and recently, at the B K edge in the recently discovered novel superconductor MgB$_2$.[9]

While organic materials composed of light elements are suited inherently well to XRS studies, inelastic X-ray scattering has not been utilized in this field to much extent. An important landmark was achieved by Bergmann and co-workers by constructing an instrument with sufficient energy resolution and a large angular acceptance of the scattered photons.[10] They demonstrated that XRS can be used as practical alternative to the XAS and the ISEELS methods in the field of aromatic hydrocarbons.[11,12] However, despite the advances in the XRS employed in the study of small organic molecules, the XRS efforts in the research of macromolecules, and electronically valuable π-conjugated polymers in particular, seem to be scarce.

Polyfluorenes (PFs)[13] are an important class of π-conjugated polymers due to their efficient optoelectronic performance and high stability. Among PFs, branched side chain poly[9,9-bis-(2-ethylhexyl)-fluorene-2,7-diyl] (PF2/6) is an important model compound as its photoluminescence and photoabsorption spectra remain largely unchanged regardless of the long-range order. Its chemical structure is relatively simple and it can be easily aligned to a high degree.[14] This makes PF2/6 also technologically interesting, as sufficient alignment results in polarized electroluminescence[15] and enhanced charge carrier mobility.[16] The self-organized structure of aligned PF2/6 has been comprehensively studied using electron diffraction,[17] fiber X-ray diffraction (XRD),[18] grazing-incidence X-ray diffraction (GIXRD),[19] and NEXAFS[20] techniques.

* Corresponding author. E-mail: szabolcs.galambosi@helsinki.fi.
† University of Helsinki.
‡ University of Durham.
§ European Synchrotron Radiation Facility.
‖ Bergische Universität Wuppertal.

In this paper, we present an XRS study on aligned PF2/6. We have two objectives: First, we extend the use of XRS to π-conjugated polymers in general and show that it is possible to make a distinction between the contributions of backbone and side groups and connect this to the macroscopic alignment of the polymer backbone, complementing diffraction and optical studies of aligned PF2/6. Moreover, we show that, in contrast to absorption methods, the momentum transfer dependence of XRS can give truly unique information about the electronic states of π-conjugated polymers. By combining the experimental data to theoretical calculations according to a very recently proposed theoretical scheme of Soininen et al.,[21] we demonstrate that the unoccupied density of electronic states can be decomposed into various symmetry components.

The energy units in this paper are in electronvolts (eV) and the momentum units are in atomic units (1 au = $1/a_0$, where a_0 is the Bohr radius).

Theoretical Section

In a nonresonant inelastic X-ray scattering (NRIXS) process, X-rays are scattered from the sample, during which some amount of energy ω and momentum $\mathbf{q}$ is transferred to the target system. Within the nonrelativistic Born approximation, the double-differential cross section for this process is given by[22]

$$\frac{d^2\sigma}{d\Omega \, d\omega_2} = \left(\frac{d\sigma}{d\Omega}\right)_{Th} S(\mathbf{q},\omega) \qquad (1)$$

The Thomson cross section $(d\sigma/d\Omega)_{Th}$ depends on the incident (scattered) photon energy ω_1 (ω_2) and polarization vector ϵ_1 (ϵ_2)

$$\left(\frac{d\sigma}{d\Omega}\right)_{Th} = r_0^2 (\epsilon_1 \cdot \epsilon_2)^2 \frac{\omega_2}{\omega_1} \qquad (2)$$

where r_0 is the classical electron radius. $S(\mathbf{q},\omega)$ is the dynamic structure factor that depends solely on the electronic characteristics of the sample.

The nonresonant condition implies that the energy of the incident photons is far from any absorption edges. However, when the energy *transfer* is close to the energy of an absorption edge (for example 285 eV for the carbon K edge), a spectral feature closely resembling an absorption edge can be observed in the scattering spectra. This process is called X-ray Raman scattering. The first experimental reports[23,24] were followed by a theoretical explanation[3] and further experimental studies[4,6] that unambiguously proved that the XRS spectrum measured at low momentum transfer values indeed gives identical information compared to that of X-ray absorption spectra.

Within the quasiparticle approximation for excitations from a tightly bound core state $|i\rangle$, the dynamic structure factor can be written as[22]

$$S(\mathbf{q},\omega) = \sum_f |\langle f | e^{i\mathbf{q}\cdot\mathbf{r}}|i\rangle|^2 \, \delta(\omega + E_i - E_f) \qquad (3)$$

where $|f\rangle$ is the photoelectron final state and E_i (E_f) is the initial (final) state energy. For small momentum transfers, the exponential in eq 3 can be expanded as

$$e^{i\mathbf{q}\cdot\mathbf{r}} \approx 1 + i\mathbf{q}\cdot\mathbf{r} + O(q^2) \qquad (4)$$

Because of the orthogonality of the initial and final states, the first term does not contribute to transitions and also the matrix elements from the quadratic q^2 (and higher terms) are small.

Thus at low momentum transfers, only the dipole allowed transitions contribute significantly to the XRS spectrum. Within this approximation, the similarity in the cross section of X-ray absorption $\sigma(\omega_1)_{XAS}$ and $S(\mathbf{q},\omega)$ of the scattering process is evident

$$\sigma(\omega_1)_{XAS} \sim \omega_1 \, |\epsilon_1 \cdot \langle f | \mathbf{r} | i\rangle|^2 \, \delta(\omega_1 + E_i - E_f) \qquad (5)$$

$$S(\mathbf{q},\omega) = |\mathbf{q}\cdot\langle f | \mathbf{r} | i\rangle|^2 \, \delta(\omega + E_i - E_f)$$

As the momentum transfer is increased, the higher-order terms in eq 4 no longer remain negligible. Thus the spectral features originating from nondipole transitions gain weight, which permits the study of electronic states not accessible with dipole transitions.

Theoretical methods for calculating the XRS spectra have been improved tremendously in recent years. Approaches such as described in refs 25,26, suitable for systems having a periodic structure, have been successfully applied in the analysis of XRS spectra from hard condensed matter systems.[7,9] For nonperiodic soft condensed matter systems, such as polymers, this approach is not applicable. Real space multiple scattering (RSMS) based methods such as the FEFF-code[27] are widely used in the analysis of XAS experiments. A very recent report[21] showed how the momentum dependence can be implemented into the RSMS framework, thus making it possible to calculate the momentum transfer dependent XRS spectra for nonperiodic systems.

For core−electron excitations, the most important source of error in the calculated XRS spectra is due to the inaccuracies in the calculated final state density of states (DOS). On the other hand, the transition matrix elements can be calculated to a relatively good accuracy. To address this problem, a new scheme was proposed by Soininen et al.,[21] in which the authors point out that, by exploiting the momentum transfer dependence of the experimental spectra together with the calculated transition matrix elements, the angular momentum projected DOS can be extracted from the data. The method is based on the fact that within a certain approximation the dynamic structure factor can be written as

$$S(\mathbf{q},\omega) \sim \sum_l c_l \, |M_l(\mathbf{q},\omega)|^2 \rho_l(\omega) \qquad (6)$$

where c_l is a coefficient, M_l is the transition matrix element, and ρ_l is the density of states having a symmetry l = s, p, d, ... This means that $S(\mathbf{q},\omega)$ at each $\mathbf{q}$ can be regarded as the linear combination of DOS having different symmetry, weighted by the relevant matrix elements. With a suitable inversion procedure the ρ_l with different symmetries can be found. The current work relies on the fact that within the dipole limit (at low q values) only contribution to $S(\mathbf{q},\omega)$ arises from p-DOS (p-orbital contribution) which can be found from the low momentum transfer spectra. At higher q values, other excitation channels start to contribute.

In comparison with optical absorption spectroscopy, the XRS method provides a direct way to examine the unoccupied density of electronic states. In XRS, the initial s-type core state combined with the dipole selection rule within the low q regime result in transitions purely into p-type unoccupied final states. In optical absorption spectroscopy, the dipole transitions also dominate, but the initial electron state is different. The deep core electron states in compounds retain their atomistic character, but the valence states can be heavily modified. In optical transitions, the initial state is formed by these valence electron states. Thus one usually cannot expect a valence state to have
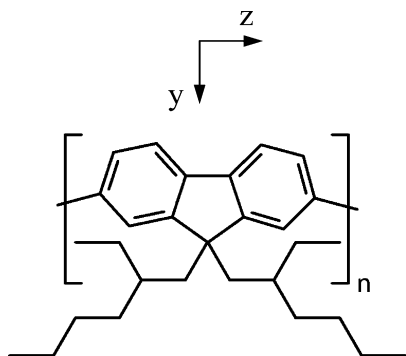
Figure 1. Chemical structure of poly[9,9-bis(2-ethylhexyl)-fluorene-2,7-diyl] (PF2/6) along with the coordinate axes used in the theoretical calculations.
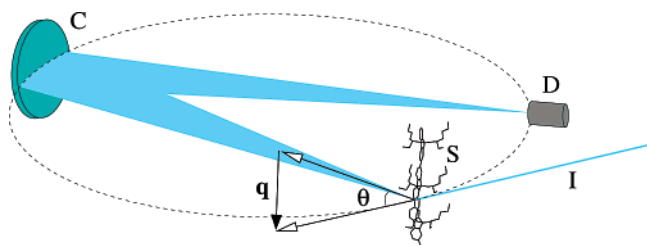

Figure 2. Experimental setup. The incident X-ray beam (I) is scattered by the sample (S). The analyzer crystal (C) focuses the scattered photons having the correct energy into the detector (D). Also shown is how the difference in the momenta of the incident and the scattered photons defines the momentum transferred (**q**) to the sample.
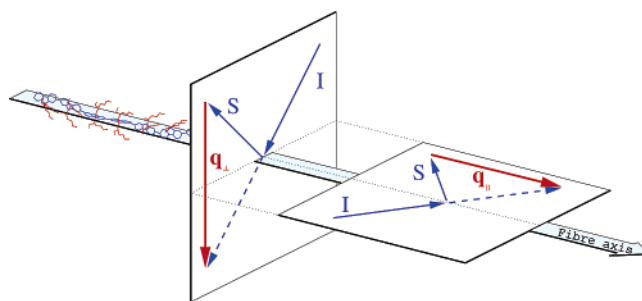

Figure 3. Schematic representation of the two measurement geometries used in the experiments. The direction of the incident (I) and scattered (S) photons relative to the fiber axis can be chosen such that the momentum transfer is either perpendicular ($q_\perp$) or parallel ($q_\parallel$) to the fiber axis.

a simple atomistic s- or p-type symmetry, which renders the study of electronic states contributing to the transitions somewhat difficult. Moreover, the density of states having other than a p-type symmetry can be extracted by employing the momentum transfer dependence of XRS.

Experimental Section

Samples. PF2/6 ($M_n = 61$ kg/mol, $M_w = 84$ kg/mol) (Figure 1) was prepared as described in ref 13. Polyfluorene fibers were drawn above the glass transition temperature as shown in ref 18. The resulting rectangular samples had the approximate dimensions of 30 mm × 7 mm × 1 mm (length × width × thickness). Each of the samples contained a large number of fibers which, in an ideal case, would have the fiber axes oriented along the longest side of the sample. The orientation distribution of the fiber axes was determined using XRD by recording the angular intensity distribution of the Debye rings using a conventional X-ray tube pinhole camera and an image plate.

Measurements. The inelastic X-ray scattering experiments were carried out on beamline ID16 at the European Synchrotron Radiation Facility (ESRF), Grenoble, France. The X-rays produced by three consecutive undulators were monochromatized using a double-crystal Si (111) monochromator. The energy of the scattered photons was selected using a spherically bent silicon crystal positioned on the Rowland circle (diameter 1 m) utilizing the Si (555) reflection in a near backscattering geometry. The experimental setup is shown schematically in Figure 2. The energy loss spectra were recorded in the so-called inverse scan technique,[28] in which the energy of the detected photons (ω_2) is kept fixed and the energy of the incident photons (ω_1) is varied. A total energy resolution of 1.3 eV was measured from the elastic line at 9885.6 eV. Two measurement geometries were used in which **q** was perpendicular or parallel to the fiber axis (Figure 3). The momentum transfer resolution Δq varied as a function of the scattering angle and was 0.21 au at $q = 1.4$

au and 0.06 au at $q = 5.13$ au, as calculated from the finite size of the analyzer crystal, which dominates the momentum resolution.

To reduce the possible degradation of the samples due to radiation damage, all X-ray scattering measurements were carried out in a vacuum and the samples were kept at a temperature of 20 K. The size of the X-ray beam at the sample was defocused to 1.5 mm × 1.5 mm. Several energy loss measurements, each lasting about 20 min, were made from the same sample, during which the consistency of the data was continuously monitored. The total measurement time was about 6 h/spectrum. The nature of radiation damage was studied further ex situ by taking photoabsorption (UV−vis and Fourier transform infrared (FTIR)), photoluminescence (PL) spectra, and XRD measurements of the radiated spots after the synchrotron experiment.

The raw experimental spectra were corrected to account for the energy dependence of the absorption occurring in the air paths, in the Kapton windows, and in the sample. The incident beam intensity was continuously monitored to account for the slowly decaying synchrotron ring current and for the energy dependence of the efficiency of the optical elements. Each measured datapoint was normalized with respect to the incident intensity and the dead-time of the detector was also taken into account. In addition to these standard corrections, the background subtraction in our case needed special attention due to other **q**- and ω-dependent electronic excitations contributing to the inelastic X-ray spectrum. In the low-q measurements, the carbon K edge was well isolated from other excitations, leading to a small linear background. For the large-q spectra, the K edge, however, resides in the middle of the valence scattering spectrum,[29] which renders the background subtraction a non-trivial task. To cope with this problem, we performed ab initio Compton scattering calculations for one monomer of PF using an extension[30] of the StoBe-DeMon package.[31] The results from the theoretical calculations reproduced the experimental Compton profile with a very good accuracy. We then felt confident to use this theoretical data to subtract the contributions of other than the carbon 1s electrons from the experimental spectra.

Computational Section

The theoretical calculations of the XRS spectra were performed using a full multiple scattering formalism program based on the FEFF8.2 package,[27] modified to produce the momentum transfer dependent X-ray Raman spectra.[21] The momentum transfer and direction dependent XRS calculations were performed for carbon atoms in the central monomer in a PF polymer consisting of three monomers. The atomic coordinates were taken from ref 32.
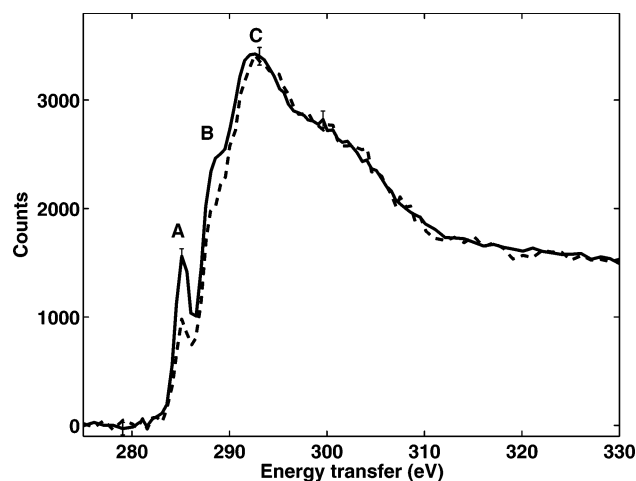
Figure 4. Background-subtracted experimental XRS spectra of oriented PF2/6 samples measured with **q** perpendicular to (solid line) and **q** along (dashed line) the drawing axis of the fibers. Selected error bars due to counting statistics are shown. Peaks A–C are described in the text.
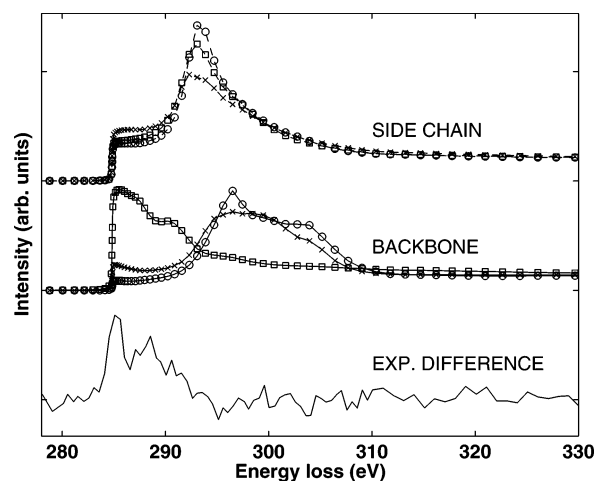

Figure 5. Calculated directional XRS spectra for a momentum transfer of 1.4 au. The upper curves represent the calculated spectra for the aliphatic side chain carbon atoms and the middle ones for the backbone carbon atoms with the momentum transfer aligned along the *x*-axis (squares), the *y*-axis (crosses), and the *z*-axis (circles). The depicted spectra represent the average over all side chain carbon atoms (dashed lines) and over all backbone carbons (solid lines). The lower curve (thin solid line) shows the difference of the experimental spectra in Figure 4.

The schematic structure of PF2/6 and coordinate system used in the calculations are shown in Figure 1. The coordinate system was chosen such that *y*- and *z*-axes are in the plane of the aromatic rings, with the latter pointing approximately along the polymer backbone. The *x*-axis is perpendicular to the planes of the aromatic rings.

In the symmetry decomposition process, the experimental data were first brought to an absolute scale by normalizing them against the calculated scattering cross section of an isolated atom.[21] By assuming that purely dipole transitions are allowed in the low-*q* spectra, the p-type DOS was found by dividing the low-*q* spectra with the calculated matrix elements. The spectral contribution of transitions to s-type states was extracted by subtracting the matrix element scaled p-DOS from the high-*q* spectra. The result was finally normalized using the proper transition matrix elements to obtain the s-DOS.

Results and Discussion

The experimental XRS spectra in the vicinity of the carbon K edge at a momentum transfer of 1.4 au in two directions are shown in Figure 4. The results can be readily compared to X-ray absorption spectra.[20] The two spectra are normalized to the same area for energies over 295 eV. The only apparent difference is the somewhat larger intensity in the 283–295 eV range when **q** is perpendicular to the drawing axis. The experimental resolution is high enough to discriminate several excitations. Peak A at around 285 eV originates from the excitation of the carbon 1s electrons into the π^* orbitals of the aromatic rings in the backbone of PF.[2,20,33–35] Feature B at about 288 eV probably originates from excitations into σ^* orbitals of the C–H bond. Peak C residing around 293 eV is assigned to transitions into σ^* states on the C–C bond.

It is well established that transitions into π^* states responsible for excitations around 285 eV (peak A) are associated with the presence of π bonds.[34] Thus in the case of PF, peak A can be uniquely identified to originate from the π-bonded carbon atoms in the aromatic rings. Other parts of the spectra are an overlap of contributions from all carbon atoms. As these π^* orbitals are highly directional, the intensity variation as a function of the scattering direction can be used to probe the orientation distribution of the π-bonded molecules.[35,36]

The peak at 285 eV is visible in both measurement geometries, suggesting that the samples had only partial orientation

preference along the drawing axis (*z*-axis). We estimated the degree of orientation by performing an XRD study on the angular intensity distribution of the (005) reflection (cf. refs 18,19). The intensity ratio of this reflection along versus perpendicular to the drawing axis was found to be 2.1:1, thus verifying that the orientation of the fibers was indeed only partial.

To gain insight into the directional dependence of the XRS spectra, we performed full multiple scattering calculations for all carbon atoms in the middle monomer of a polyfluorene polymer consisting of three monomer units. The calculated directional low-momentum transfer XRS spectra averaged over the backbone carbon atoms and over the aliphatic atoms are shown in Figure 5. It is strikingly visible that the directional dependence is predicted to be almost totally due to the backbone carbons, namely the difference between the *yz*-plane and the *x*-direction. In a polyfluorene polymer, the consecutive monomers are rotated relative to each other around the *z*-axis.[18,19] This means that, even if we can define the *z*-direction accurately, the physical properties perpendicular to this axis can be regarded as an angular average of the *xy*-plane. Thus by measuring the XRS spectra along the polymer drawing axis, one should probe mainly the electronic properties along the *z*-direction. On the other hand, with **q** perpendicular to the drawing axis, one studies the properties averaged in the *xy*-plane. We exploit the meridional orientation of our samples by taking the difference of the spectra in Figure 4, i.e., the spectra measured along the drawing axis and perpendicular to it. As shown in the lower part of Figure 5, the difference spectrum is found to correlate very well with the theoretically calculated XRS spectrum projected along the *x*-axis for the backbone atoms. From the calculated spectrum, it is evident that for polyfluorene FEFF8.2 does not reproduce the sharp peak at 285 eV. Thus, while qualitatively it is clear that most of the direction dependence is due to the difference between the *x*- and *z*-directions for the backbone atoms, quantitative conclusions from the fine structures should not be drawn.

The momentum transfer dependence of the XRS spectrum is shown in Figure 6. The integrated intensity of the XRS spetrum grows quickly with increasing *q*.[37] To emphasize the differences
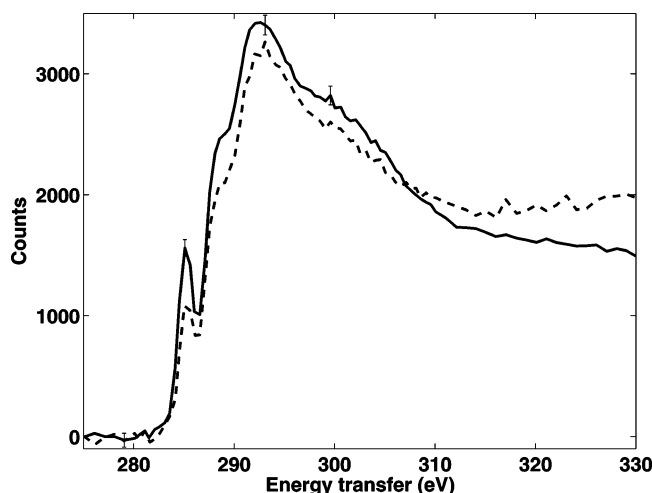
Figure 6. XRS spectrum of PF with **q** perpendicular to the drawing axis at 1.4 au (solid line) and 5.13 au (dashed line).
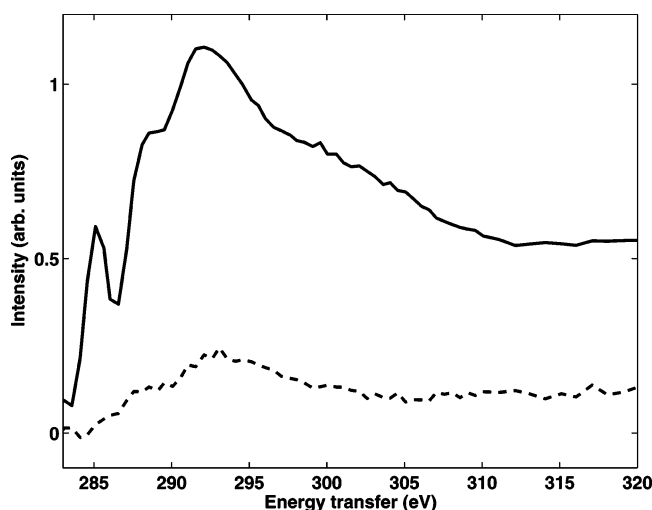

Figure 7. Final state angular momentum projected density of states of PF2/6 showing the *s*-DOS (dashed line), *p*-DOS (solid line).

of the spectra, the data shown here are normalized to the same area as is done in XAS.[38] The changes in the spectrum are subtle, but we would like to point out that the differences are due to the changes in the transition matrix elements. The spectrum can no longer be regarded as originating purely from dipole-allowed transitions. From Figure 6, it is evident that the higher-energy regions gain considerable weight when compared to the near-edge region. Especially, the relative intensity of the 285 eV peak is greatly diminished when compared to the maximum of the spectrum.

We carried out also XAS calculations using the FEFF8.2 program[27] and compared them to our calculated XRS spectra at $q = 1.4$ au. We found the two spectra virtually identical, confirming that the low momentum transfer XRS spectra can be regarded as originating from pure dipole allowed transitions from an s-type core state to p-type valence states. Using the calculated matrix elements together with the high momentum transfer spectrum, we can find the s-type density of final states. Our main result is shown in Figure 7. According to Figures 5 and 7, the peak at 285 eV is due to electronic states that are perpendicular to the aromatic rings having a pure p-type symmetry. These perpendicular states span to about 10 eV over the edge with a slightly increasing s-symmetry character. All other electronic states have, to some extent, an s-type character along with the dominating p-type symmetry. The largest
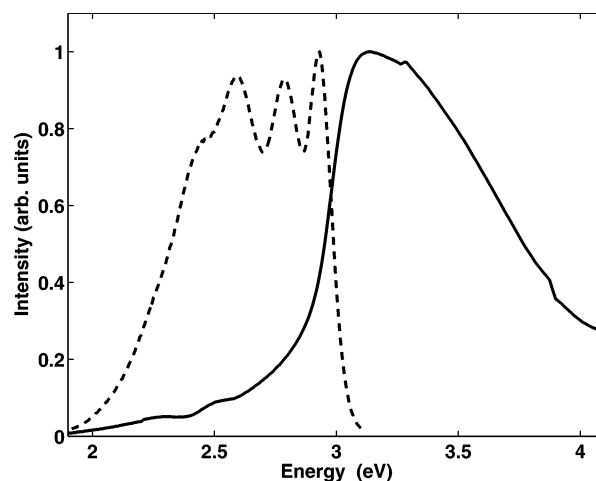

Figure 8. Photoluminescence (left) and absorption (right) spectra from the irradiated part of PF2/6. A small kink in the absorption spectrum at 3.3 eV is an artifact from the spectrometer.

contribution to the s-DOS happens around 293 eV, coinciding with the maxima in the calculated XRS spectra for the side chain carbon atoms.

Now, compared to XANES, the extra information contributed by XRS is evident. Not only can the equivalent of the absorption spectra be measured using hard X-rays, but the symmetry of the states leading to the various spectral features can readily be found. In this context, it is intriguing to note that the pure p-type symmetry of the states at 285 eV are in an excellent accord with what one would expect from the simple Hückel molecular orbital model for the π orbitals.

As described earlier in the Experimental Section, the measurements were carried out in a vacuum environment at low temperatures with a defocused beam in order to reduce the radiation damage to the samples. Despite these measures, after about 10 min of exposure, a slight darkening of the irradiated part of the sample could be observed. As the data collection consisted of several 20−30 min scans, we felt the need to investigate the possible degradation of the samples.

We performed several quick (2−3 min) XRS scans at the carbon K edge, moving the footprint of the beam to a fresh spot for each scan. The sum of the data from these scans were indistinguishable from the actual data collection scans within counting statistics. We also measured the valence excitation spectra both with shorter and longer measurement times, but could not detect any time dependence of the spectra in this case either. We thus concluded that either the possible degradation is such that the current method is insensitive to it or the sample degradation due to radiation damage occurs on a time scale shorter than 2 min.

The intense X-ray beam is, however, expected to partially ionize the polymer, which may result in cross linking. This probably explains the observed reduction in the solubility of the polymer, which made the molecular weight determination with gel permeability chromatography (GPC) impractical. A 10 nm red-shift of the photoluminescence maximum (from 370−385 nm to 380−395 nm) as well as an additional green emission component beneath the original 0−0 and 0−1 peaks of the polyfluorene PL spectrum were also observed. An example of these spectra is shown in Figure 8. As the FTIR spectrum did not indicate the presence of fluorenone groups, we expect that the additional PL bands at 2.6/2.4 eV are predominantly not due to well-known keto defects.[39] These bands are not related to cross linking either, as simple cross linking of the side chains will not result in colored products. They may be an indication

of dibenzofulvene defects, which are formed in a sequence of two electron transfer and deprotonation steps in the absence of oxygen.[40,41] It is yet noteworthy that the spectra shown in Figure 8 represent the worst case scenario after all exposures and they are still dominated by the contribution of the defect-free polyfluorene.

X-ray diffraction spectra from the irradiated part of the samples showed a somewhat decreased intensity of the diffraction maxima and higher amorphous background when compared to the pristine sample spots. However, the angular distribution of the diffraction maxima were unaltered.

From these studies, we argue that the radiation damage does not impede the successful interpretation of XRS data. The colorization of the samples is not due to the well-known keto defects or simple cross linking. It may arise from nonoxidatively formed dibenzofulvene moieties. These defects apparently affect the crystallinity of the sample, but they do not alter the orientational distribution of the polymers.

Conclusions

In summary, we have conducted an XRS study of aligned PF2/6 and qualitatively interpreted the spectra based on the theoretical framework. In particular, we have shown that it is possible to make a distinction between the contributions of backbone and side group carbon atoms. Moreover, we have shown that the highly directional nature of the electronic states of the aromatic carbon groups makes it possible to study the orientation of π-conjugated polymers via XRS, thus complementing XAS, XRD, and optical studies to some extent. We have also demonstrated that the momentum transfer dependence of the XRS spectrum can be utilized to find angular momentum projected density of states.

References and Notes

(1) Wende, H. *Rep. Prog. Phys.* **2004**, *67*, 2105−2181.
(2) Stöhr, J. In *NEXAFS Spectroscopy*; Gomer, R., Ed.; Springer Series in Surface Sciences 25; Springer-Verlag: Berlin, 1992.
(3) Mizuno, Y.; Ohmura, Y. *J. Phys. Soc. Jpn.* **1967**, *22*, 445−449.
(4) Tohji, K.; Udagawa, Y. *Phys. Rev. B* **1989**, *39*, 7590−7594.
(5) Bowron, D. T.; Krisch, M. H.; Barnes, A. C.; Finney, J. L.; Kaprolat, A.; Lorenzen, M. *Phys. Rev. B* **2000**, *62*, R9223−R9227.
(6) Nagasawa, H.; Mourikis, S.; Schülke, W. *J. Phys. Soc. Jpn.* **1989**, *58*, 710−717.
(7) Hämäläinen, K.; Galambosi, S.; Soininen, J. A.; Shirley, E. L.; Rueff, J.-P.; Shukla, A. *Phys. Rev. B* **2002**, *65*, 155111.
(8) Sternemann, C.; Volmer, M.; Soininen, J. A.; Nagasawa, H.; Paulus, M.; Enkisch, H.; Schmidt, G.; Tolan, M.; Schülke, W. *Phys. Rev. B* **2003**, *68*, 035111.
(9) Mattila, A.; Soininen, J. A.; Galambosi, S.; Huotari, S.; Vankó, G.; Zhigadlo, N. D.; Karpinski, J.; Hämäläinen, K. *Phys. Rev. Lett.* **2005**, *94*, 247003.
(10) Bergmann, U.; Glatzel, P.; Cramer, S. P. *Microchem. J.* **2002**, *71*, 221−230.
(11) Gordon, M. L.; Tulumello, D.; Cooper, G.; Hitchcock, A. P.; Glatzel, P.; Mullins, O. C.; Cramer, S. P.; Bergmann, U. *J. Phys. Chem. A* **2003**, *107*, 8512−8520.
(12) Bergmann, U.; Groenzin, H.; Mullins, O. C.; Glatzel, P.; Fetzer, J.; Cramer, S. P. *Chem. Phys. Lett.* **2003**, *369*, 184−191.
(13) Scherf U.; List, E. J. W. *Adv. Mater.* **2002**, *14*, 477−487.
(14) Knaapila, M.; Stepanyan, R.; Lyons, B. P.; Torkkeli, M.; Monkman, A. P. *Adv. Funct. Mater.* **2006**, *16*, 599−609.
(15) Grell, M.; Knoll, W.; Lupo, D.; Meisel, A.; Miteva, T.; Neher, D.; Nothofer, H.-G.; Scherf, U.; Yasuda, A. *Adv. Mater.* **1999**, *11*, 671−675.
(16) Yasuda, T.; Fujita, K.; Tsutsui, T.; Geng, Y.; Culligan, S. W.; Chen, S. H. *Chem. Mater.* **2005**, *17*, 264−268.
(17) Lieser, G.; Oda, M.; Miteva, T.; Meisel, A.; Nothofer, H.-G.; Scherf, U.; Neher, D. *Macromolecules* **2000**, *33*, 4490−4495.
(18) Knaapila, M.; Stepanyan, R.; Torkkeli, M.; Lyons, B. P.; Ikonen, T. P.; Almásy, L.; Foreman, J. P.; Serimaa, R.; Güntner, R.; Scherf, U.; Monkman, A. P. *Phys. Rev. E* **2005**, *71*, 041802.
(19) Knaapila, M.; Stepanyan, R.; Lyons, B. P.; Torkkeli, M.; Hase, T. P. A.; Serimaa, R.; Güntner, R.; Seeck, O. H.; Scherf, U.; Monkman, A. P. *Macromolecules* **2005**, *38*, 2744−2753.
(20) Jung, Y.; Cho, T.-Y.; Yoon, D. Y.; Frank, C. W.; Lüning, J. *Macromolecules* **2005**, *38*, 867−872.
(21) Soininen, J. A.; Ankudinov, A. L.; Rehr, J. J. *Phys. Rev. B* **2005**, *72*, 045136.
(22) Schülke, W. In *Handbook on Synchrotron Radiation*; Brown, G. S., Moncton, D. E., Eds.; Elsevier Science Publishers: Amsterdam, 1991; Vol. 3, pp 565−637.
(23) Das Gupta, K. *Phys. Rev. Lett.* **1959**, *3*, 38−40.
(24) Suzuki, T. *J. Phys. Soc. Jpn.* **1967**, *22*, 1139−1150.
(25) Soininen, J. A.; Caliebe, W. A.; Shirley, E. L.; Kao, C.-C.; Hämäläinen, K. *J. Phys: Condens. Matter* **2001**, *13*, 8039−8047.
(26) Soininen, J. A.; Shirley, E. L. *Phys. Rev. B* **2001**, *64*, 165112.
(27) Ankudinov, A. L.; Ravel, B.; Rehr, J. J.; Conradson, S. D. *Phys. Rev. B* **1998**, *58*, 7565−7576.
(28) Hämäläinen, K.; Manninen, S.; Kao, C.-C.; Caliebe, W.; Hastings, J. B.; Bansil, A.; Kaprzyk, S.; Platzman, P. M. *Phys. Rev. B* **1996**, *54*, 5453−5459.
(29) Cooper, M. J.; Mijnarends, P. E.; Shiotani, N.; Sakai, N.; Bansil, A. In *X-ray Compton Scattering*; Chikawa, J., Helliwell, J. R., Lovesey, S. W., Eds.; Oxford Series on Synchrotron Radiation 5; Oxford University Press: Oxford, 2004.
(30) Hakala, M.; Huotari, S.; Hämäläinen, K.; Manninen, S.; Wernet, Ph.; Nilsson, A.; Pettersson, L. G. M. *Phys. Rev. B* **2004**, *70*, 125413.
(31) Hermann, K.; Pettersson, L. G. M.; Casida, M. E.; Daul, C.; Goursot, A.; Koester, A.; Proynov, E.; St-Amant, A.; Salahub, D. R.; Carravetta, V.; Duarte, H.; Godbout, N.; Guan, J.; Jamorski, C.; Leboeuf, M.; Malkin, V.; Malkina, O.; Nyberg, M.; Pedocchi, L.; Sim, F.; Triguero, L.; Vela, A. *StoBe-deMon*, version 1.0; StoBe Software, 2002.
(32) Knaapila, M.; Kisko, K.; Lyons, B. P.; Stepanyan, R.; Foreman, J. P.; Seeck, O. H.; Vainio, U.; Pålsson, L.-O.; Serimaa, R.; Torkkeli, M.; Monkman, A. P. *J. Phys. Chem. B* **2004**, *108*, 10711−10720.
(33) Ågren, H.; Vahtras, O.; Carravetta, V. *Chem. Phys.* **1995**, *196*, 47−58.
(34) Dhez, O.; Ade, H.; Urquhart, S. G. *J. Electron Spectrosc. Relat. Phenom.* **2003**, *128*, 85−96.
(35) Pattison, L. R.; Hexemer, A.; Kramer, E. J.; Krishnan, S.; Petroff, P. M.; Fischer, D. A. *Macromolecules* **2006**, *39*, 2225−2231.
(36) Stöhr, J.; Outka, D. A. *Phys. Rev. B* **1987**, *36*, 7891.
(37) Schülke, W.; Bonse, U.; Nagasawa, H.; Kaprolat, A.; Berthold, A. *Phys. Rev. B* **1988**, *38*, 2112.
(38) Wernet, Ph.; Nordlund, D.; Bergmann, U.; Cavalleri, M.; Odelius, M.; Ogasawara, H.; Näslund, L. Å.; Hirsch, T. K.; Ojamäe, L.; Glatzel, P.; Pettersson, L. G. M.; Nilsson, A. *Science* **2004**, *304*, 995.
(39) Hintschich, S. I.; Rothe, C.; Sinha, S.; Monkman, A. P.; Scandiucci de Freitas, P.; Scherf, U. *J. Chem. Phys.* **2003**, *119*, 12017−12022.
(40) Nakano, T.; Takewaki, K.; Yade, T.; Okamoto, Y. *J. Am. Chem. Soc.* **2001**, *123*, 9182−9183.
(41) Monkman, A. P., Burrows, H., Tretiak, S., Galbrecht, F., Scherf, U. Manuscript in preparation.